Journal of Applied Polymer Science

Effects of Surface Modification of Carbon Nanofibers on the Mechanical Properties of Polyamide 1212 Composites

Ziqing Cai,[1,2] Xiaoyu Meng,[1,2] Xiaocan Zhang,[1,2] Lishan Cui,[1,2] Qiong Zhou[1,2]

[1]Department of Materials, College of Science, China University of Petroleum, Beijing 102249, China

[2]Beijing Key Laboratory of Failure, Corrosion, and Protection of Oil/Gas Facilities, China University of Petroleum, Beijing 102249, China

Correspondence to: X. Meng (E-mail: xymeng800418@sohu.com) and Q. Zhou (E-mail: cuppolymer@163.com)

ABSTRACT: In this study, the effects of carbon nanofiber (CNF) surface modification on mechanical properties of polyamide 1212 (PA1212)/CNFs composites were investigated. CNFs grafted with ethylenediamine (CNF-*g*-EDA), and CNFs grafted with polyethyleneimine (CNF-*g*-PEI) were prepared and characterized. The mechanical properties of the PA1212/CNFs composites were reinforced efficiently with addition of 0.3 wt % modified CNFs after drawing. The reinforcing effect of the drawn composites was investigated in terms of interfacial interaction, crystal orientation, crystallization properties and so on. After the surface modification of CNFs, the interfacial adhesion and dispersion of CNFs in PA1212 matrix were improved, especially for CNF-*g*-PEI. The improved interfacial adhesion and dispersion of CNFs in PA1212 matrix was beneficial to reinforcement of the composites. Compared with pure PA1212, improved degree of crystal orientation in the PA1212/CNF-*g*-PEI (CNF-*g*-EDA) composites was responsible for reinforcement of mechanical properties after drawing. © 2014 Wiley Periodicals, Inc. J. Appl. Polym. Sci. **2015**, *132*, 41424.

KEYWORDS: composites; graphene and fullerenes; mechanical properties; nanotubes; polyamides

Received 10 June 2014; accepted 20 August 2014

DOI: 10.1002/app.41424

INTRODUCTION

Carbon nanofibers and nanotubes have the similar structures.[1,2] They are widely used in the reinforcement of semi-crystalline polymers based on their excellent properties, such as high mechanical strength/modulus,[3] large specific surface area/aspect ratio[4] and so on. However, reinforcing effect of nanofillers is not significant as expected.[5] The restraining factors include inadequate dispersion and alignment of the nanofillers, poor adhesion and load transfer at interfaces.[5] To improve the dispersion state and interfacial adhesion, the surface modification of CNTs/CNFs is essential.[6,7] Meng et al.[8] prepared PA6/MWNTs composites with acid- and diamine-modified MWNTs by a simple melt compounding method. Better dispersion and stronger interfacial adhesion of diamine-modified MWNTs in PA6 matrix could be obtained. Mechanical properties of the composites were improved significantly with the addition of the diamine-modified MWNTs. Shi et al.[9] reported that an interfacial layer existed outside modified CNFs in polystyrene composites. The interfacial layer caused by surface modification enhanced the dispersion and interfacial adhesion of CNFs in polymer matrix.

The alignment of CNTs/CNFs and polymer chain orientation in the composites can be realized by subsequent stretching or drawing after molding.[10,11] This method is often used to improve the mechanical properties of the composites.[12,13] During the aligning process of nanofibers, the oriented interphase is formed on the surfaces of nanofibers.[14,15] The interphase promotes the load transfer between nanofibers and polymer matrix and it exhibits higher mechanical properties than virgin polymer.[16,17] Thereby, the reinforcing effect of nanofibers in composites can be completed during uniaxial drawing process. The effect of nanofiber surface modification on the formation of interfacial layer is a very important issue in the reinforcement of polymer composites.

Meanwhile, the degree of polymer chain orientation is influenced by the addition of CNTs/CNFs. CNTs/CNFs show obvious heterogeneous nucleation effect in polymer matrix,[18,19] polymer chains epitaxially crystallize on the surface of nanofibers,[20–22] and then the relaxation of polymer chains is hindered.[13,20] Further, the surface modification of nanofillers will enhance polymer chains orientation effectively due to the improved interfacial adhesion and dispersion in polymer matrix.[23] More polymer chains experience force along load direction, as the degree of polymer chain orientation is increasing.[11,24] Then improving degree of polymer chain orientation is another way of reinforcing the composites. Consequently, the effect of nanofiber surface modification on polymer chain orientation during drawing process is an important topic. However, the literatures about this topic are very few.

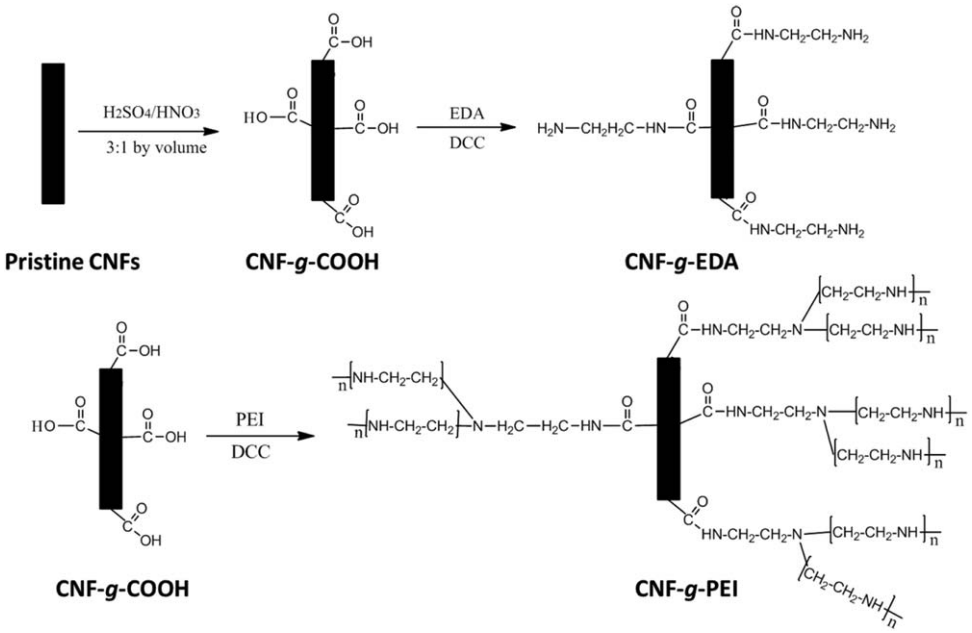

Figure 1. The schematic diagram for the preparation of CNF-*g*-EDA and CNF-*g*-PEI.

In this study, CNFs were modified by covalent grafting of two different molecules (EDA and PEI). Polyamide 1212 was used as the matrix materials and PA1212/CNFs composites with different CNF contents were prepared by melt blending. The oriented specimens were prepared by drawing at 170°C (near the melting temperature of PA1212) at 380% engineering strain. The CNFs and polymer chains were aligned and oriented during the drawing process. The effect of CNF surface modification on mechanical properties and structural evolution was investigated. The reinforcing effect in composites was analyzed associated with three different surface states of CNFs.

EXPERIMENTAL

Materials

PA1212 pellets (MI = 3.75 g/10 min) were purchased from Shandong Dongcheng Engineering Plastic. Pristine CNFs with main diameter ranging from 50 to 150 nm and length ranging from 10 to 30 μm (>95% purity) were purchased from Beijing Dekei Daojin Nanotechnology. Polyethyleneimine (PEI) (>99% purity, $M_w = 1800$) and *N*,*N*′-dicyclohexylcarbodiimide (DCC) (>99% purity, $M_w = 206$) were both supplied by Aladdin Chemistry. Concentrated sulfuric acid (H_2SO_4), concentrated nitric acid (HNO_3), ethylenediamine (EDA) and *N*,*N*′-dimethyl formamide (DMF) were supplied by Beijing Chemical Company.

Modification of CNFs

Pristine CNFs were dispersed in concentrated H_2SO_4/HNO_3 (3 : 1 v/v) solution in an ultrasonic bath (40 kHz, 200 W) for 30 min, and then mechanically stirred at 60°C for 4 h. The dispersion solution was then diluted with large quantity of water and washed with deionized water for several times until the pH of the solution reached 7.0. The CNFs were dried at 80°C in a vacuum environment for 24 h, resulting in CNFs modified with carboxylic acid groups (CNF-*g*-COOH).

CNF-*g*-COOH (1.0 g) and DCC (0.5 g) were mixed with EDA (200 mL) and the solution was refluxed at 125°C for 24 h, resulting in CNFs grafted with EDA molecules (CNF-*g*-EDA). CNF-*g*-COOH (1.0 g), DCC (0.5 g), and PEI (0.5 g) were mixed with DMF (200 mL) and the solution was refluxed at 165°C for 24 h, to produce CNFs grafted with PEI molecules (CNF-*g*-PEI).

The products were washed with ethanol to remove residual modifying agent, and then dried at 80°C for 24 h. The schematic diagram for surface modification of CNFs is shown in Figure 1. The pristine CNFs and modified CNFs were characterized by scanning electron microscopy (SEM), Fourier transform infrared (FTIR) spectroscopy, and thermogravimetric analysis (TGA).

Preparation of PA1212/CNFs Composites

Before melt blending, PA1212 pellets and CNFs were dried at 80°C for 24 h in a vacuum oven. Composites with three kinds of CNFs (pristine CNFs, CNF-*g*-EDA and CNF-*g*-PEI, 0.3 wt % content) were prepared by melt blending in a Brabender mixer (40 rpm) at 205°C for 12 min. Plate specimens (1.2 ± 0.2 mm thickness) were prepared by compression molding at 210°C for 10 min. The drawing dumbbell specimens were cut by the cutting mold, and the mold size is 4 ± 0.2 mm width, and 75 ± 1.0 mm length. Uniaxial drawing process was performed using an electronic universal tensile testing machine. The dumbbell specimens were inserted in a high temperature oven and equilibrated at 170°C for 5 min. To prepare oriented specimens, the drawing strain was set at 380% and 50 mm min^{-1} speed. The specimens were cooled to room temperature.

Performance Testing and Structural Characterization

FTIR (Nicolet 470) spectroscopy was used to characterize the functional groups on CNFs. The samples were mixed with KBr

to prepare KBr/CNFs disks. The spectra were measured between 400 and 4000 cm^{-1}, and the resolution was set at 4 cm^{-1}.

TGA (TG 209) was employed to characterize the grafting degree under argon atmosphere. TGA curves were obtained at temperatures ranging from 20 to 800°C at 10°C min^{-1} heating rate.

Raman spectrum measurement was conducted using a JY/Horiba XploRA Raman system, which equipped with 532.06 nm (frequency doubled Nd:YAG) laser excitation, a 20 Olympus objective with 0.25 numerical aperture, and a 600-groove/mm grating with a spectral resolution of ~1 cm^{-1}. Approximately 20 mW laser light was focused on the surface of the samples during the measurement. The PA1212 composites containing 10 wt % CNFs were prepared for Raman analysis.

The mechanical properties of the samples were determined using an electronic universal tensile testing machine. The tensile strength, Young's modulus and elongation at breakage point were measured at room temperature at 50 mm min^{-1}.

The thermal properties of the samples were determined by differential scanning calorimetry (DSC 204 F1, NETZSCH) under argon atmosphere. For non-isothermal melt crystallization, the samples were heated from 25 to 220°C at 10°C min^{-1} rate, held for 2 min to remove thermal history, and then cooled down to 25°C. The melting-crystallization points (T_m and T_c) and crystallinity (X_c) were determined. To obtain glass transition temperature (T_g), the samples were quenched in ethanol after melting and heated from −20 to 100°C at 20°C min^{-1} rate.

Two-dimensional WAXD (2D-WAXD) experiments were conducted using a Rigaku R-Axis Spider diffractometer at room temperature, and the wavelength of the monochromated X-ray from Mo radiation was 0.0708 nm. The samples were placed at an orientation (drawing direction) perpendicular to the projection beam. The orientation degree of the (100) crystal plane was calculated by Herman's orientation function:

$$f = \frac{3\langle \cos^2 \phi \rangle - 1}{2} \quad (1)$$

$$\cos^2 \varphi = \frac{\int_0^{\pi/2} I(\varphi) \sin \varphi \cos^2 \varphi d\varphi}{\int_0^{\pi/2} I(\varphi) \sin \varphi d\varphi} \quad (2)$$

where φ is the average angle between the normal of the given (100) crystal plane and the drawing direction.

The undrawn samples were fractured in liquid nitrogen, and the fracture surfaces were used to observe the dispersion morphology of the composites. The fracture surfaces were covered with a thin layer of gold, and the morphology was observed by SEM (Quanta 200F) operated at 20 kV. The morphology of CNFs was characterized by SEM instrument and TEM instrument (FEI F20).

RESULTS AND DISCUSSION

Characterization of CNFs and PA1212/CNFs Composites

To improve the dispersion and interfacial adhesion of CNFs in PA1212 matrix, surface modification of CNFs is necessary. Given that CNFs have C—C and C═C structures similar to CNTs, strong acid oxidation can be employed for surface modification. The functional groups including —COOH and —OH can be introduced to the surface of CNFs, and the CNFs can be modified by reactive grafting of EDA and PEI molecules.[25] The morphology of pristine CNFs is shown in Figure 2(a,d), and CNFs exhibit smooth surface. However, as shown in Figure 2(b,e), the morphology of CNF-*g*-EDA is different; they exhibit rough surface and shorter length after modification. The morphology of CNF-*g*-PEI is similar to CNF-*g*-EDA [Figure 2(c,f)], and the rough suface of CNF-*g*-PEI is also attributed to the wrapped PEI molecules on the CNFs.

From Figure 3(a), the FTIR spectrum of pristine CNFs exhibit typical C═C stretching bands at 1567 cm^{-1}, which corresponds to the graphene structure.[26] In the FTIR spectrum of the CNF-*g*-COOH, the peak at 1712 cm^{-1} is attributed to the C═O stretching vibrations of the carboxylic group (COOH), and the peak at 3425 cm^{-1} is attributed to the O—H stretching vibrations on the surface of CNFs.[27] For CNF-*g*-EDA, the band around 1655 cm^{-1} is assigned to stretching vibrations of C═O in amide group, indicating that EDA molecules are grafted on the surface of CNFs. The band around 1712 cm^{-1} is assigned to stretching vibrations of residual C═O which had not reacted with EDA molecules. For CNF-*g*-PEI, the band around 1655 cm^{-1} is assigned to stretching vibrations of C═O in amide group. It indicates that PEI molecules are grafted on the surface of CNFs via covalent bonding.

As shown in Figure 3(b), for pristine CNFs, the weight loss of accelerates at ~175–480°C, and the weight loss is ~4.5 wt %. For CNF-*g*-EDA and CNF-*g*-PEI, the weight loss increases ~200–490°C. The weight loss indicates that EDA and PEI molecules fall off from the surfaces of CNFs and then decompose at higher temperature. The calculated grafting degree of CNF-*g*-EDA and CNF-*g*-PEI is ~17.4 wt % and ~28.5 wt %, respectively.

As shown in Figure 4(a), CNFs in all samples show three distinct resonance bands (D, G, and G′ bands) in Raman spectrum. The D band is assigned to structural disorder resonance coming from amorphous carbon and defects.[28] The G band originates from the tangential in-plane stretching vibrations of the sp^2 carbon–carbon bonds within the lattice structure.[28] The G' band is the second-order vibration mode which is the overtone of the D band. For PA1212/pristine CNFs composite, the positions of D and G bands almost have no change compared with pristine CNFs powders. It indicates that there is poor interfacial adhesion between pristine CNFs and PA1212 matrix. For PA1212/CNF-*g*-EDA (CNF-*g*-PEI) composites, the positions of D and G′ bands appears a blue-shift (about 10 cm^{-1}) and it can be speculated that the interfacial adhesion between CNFs and polymer matrix is stronger compared with PA1212/pristine CNFs composite.[29]

The glass transition temperature (T_g) can effectively represent the mobility of polymer chains. In polymer composites, when the favorable interface is formed between polymer matrix and nanofillers, the mobility of polymer chains at the interface can be hindered, and then T_g is changed. As presented in Figure 4(b), the T_g of pure PA1212 is ~44.0°C. With the addition of

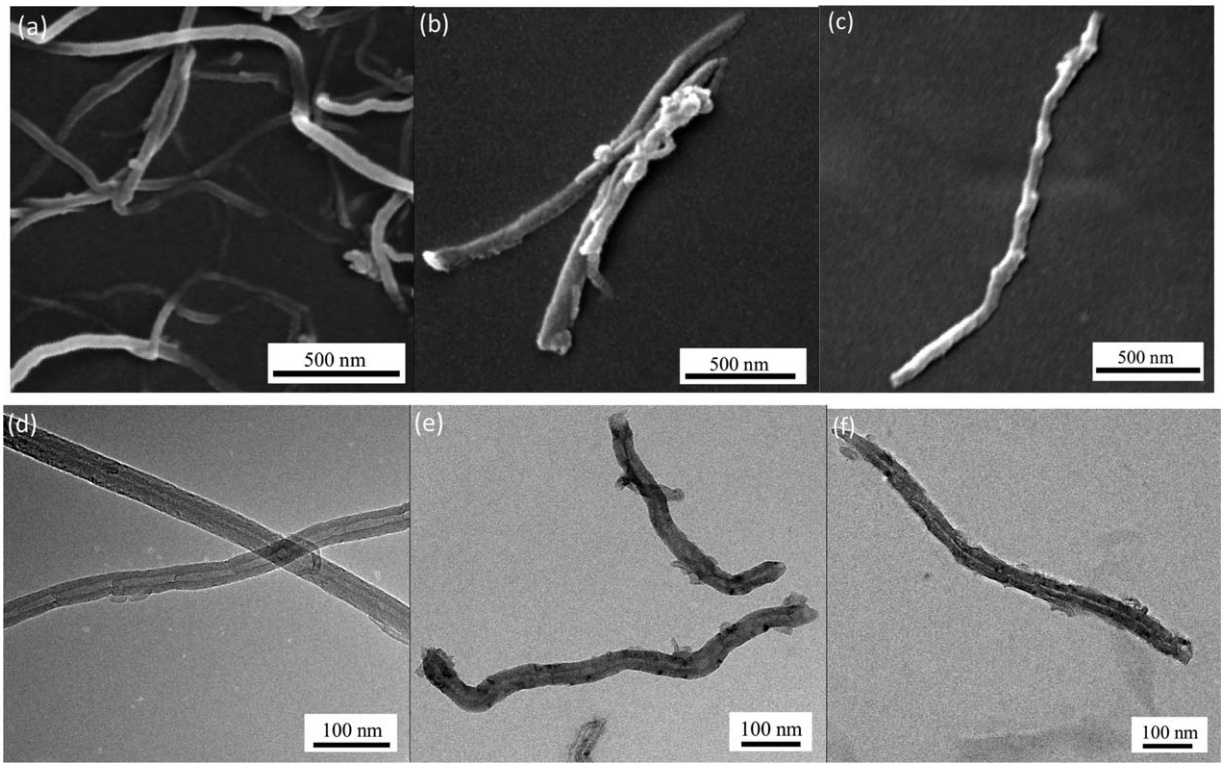

Figure 2. SEM and TEM images of pristine CNFs (a) and (d), CNF-*g*-EDA (b) and (e), CNF-*g*-PEI (c) and (f).

0.3 wt % pristine CNFs, T_g of the composite is ~43.4°C and is slightly lower compared with pure PA1212. For the composites containing 0.3 wt % CNF-*g*-EDA and CNF-*g*-PEI, T_g increases to ~45.2 and ~47.8°C respectively. It indicates that the mobility of PA1212 molecule chains can be restrained at the interface with the addition of modified CNFs. The favorable interfacial adhesion also can be proved by Raman spectrum results.

As shown in Figure 5(a), the pristine CNFs aggregate in the composite, which indicates poor dispersion ability and weak interfacial adhesion between pristine CNFs and PA1212 matrix. Given that CNFs are grafted with EDA and PEI molecules, the favorable dispersion of CNFs in the composites is completed due to the strong interfacial bonding strength. For PA1212/CNF-*g*-EDA composite, CNF-*g*-EDA can be well dispersed in PA1212 matrix [in Figure 5(b)]. As shown in Figure 5(c), CNF-*g*-PEI particles are more uniformly dispersed in the composite. Some of the CNF-*g*-PEI and CNF-*g*-EDA are broken apart in the PA1212 matrix before being pulled out. These observations suggest that CNF-*g*-PEI/CNF-*g*-EDA and PA1212 matrix exhibit good compatibility and interfacial adhesion.

Mechanical Properties of Pure PA1212 and PA1212/CNFs Composites

The relationship between the mechanical properties of the composites and three kinds of CNFs is shown in Figure 6. For the

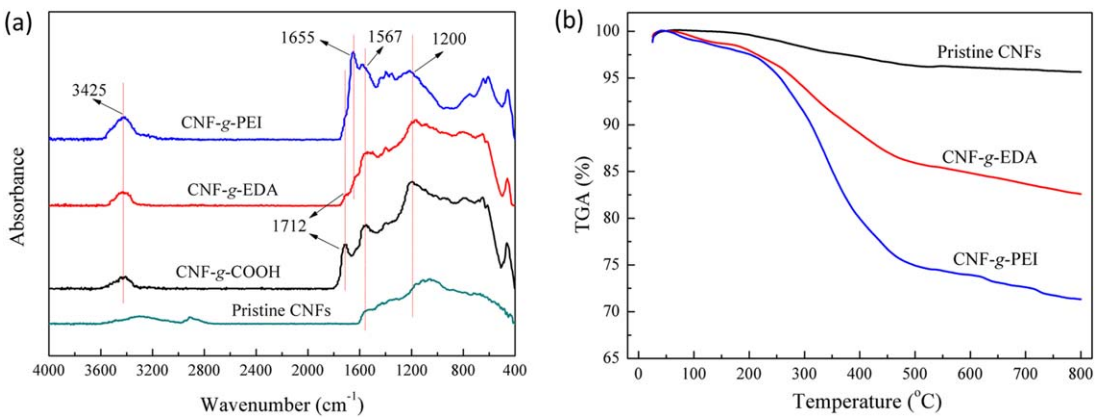

Figure 3. (a) FTIR spectra and (b) TGA curves of pristine CNFs, CNF-*g*-EDA and CNF-*g*-PEI. [Color figure can be viewed in the online issue, which is available at wileyonlinelibrary.com.]

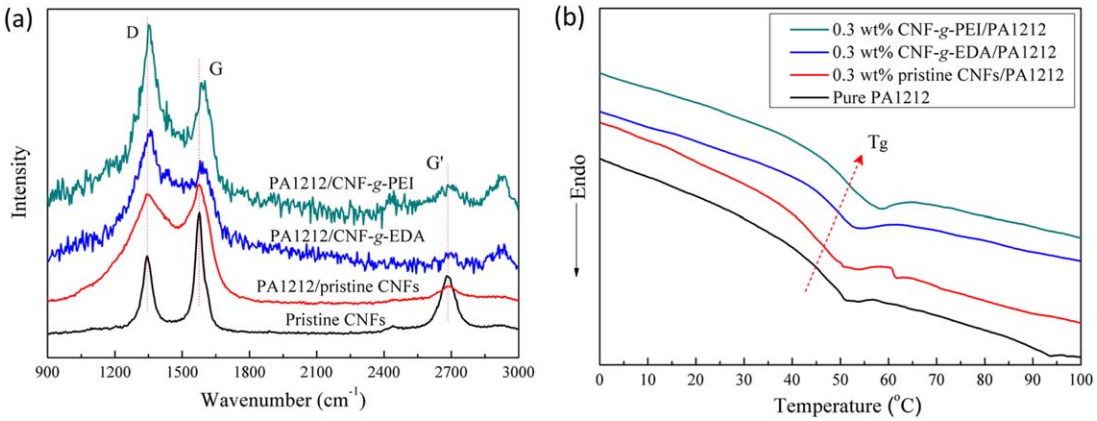

Figure 4. (a) Raman spectrum of pristine CNFs powders and PA1212/CNFs composites and (b) the glass transition temperature of pure PA1212 and PA1212/CNFs composites. [Color figure can be viewed in the online issue, which is available at wileyonlinelibrary.com.]

undrawn PA1212/pristine CNFs composite, the tensile strength and elongation at break decrease significantly with the addition of CNFs [Figure 6(a)]. From the morphology of pristine CNFs in the composite in Figure 5(a), it can be speculated that the structure defects originated from aggregation of CNFs lead to the decrease of mechanical properties. The mechanical

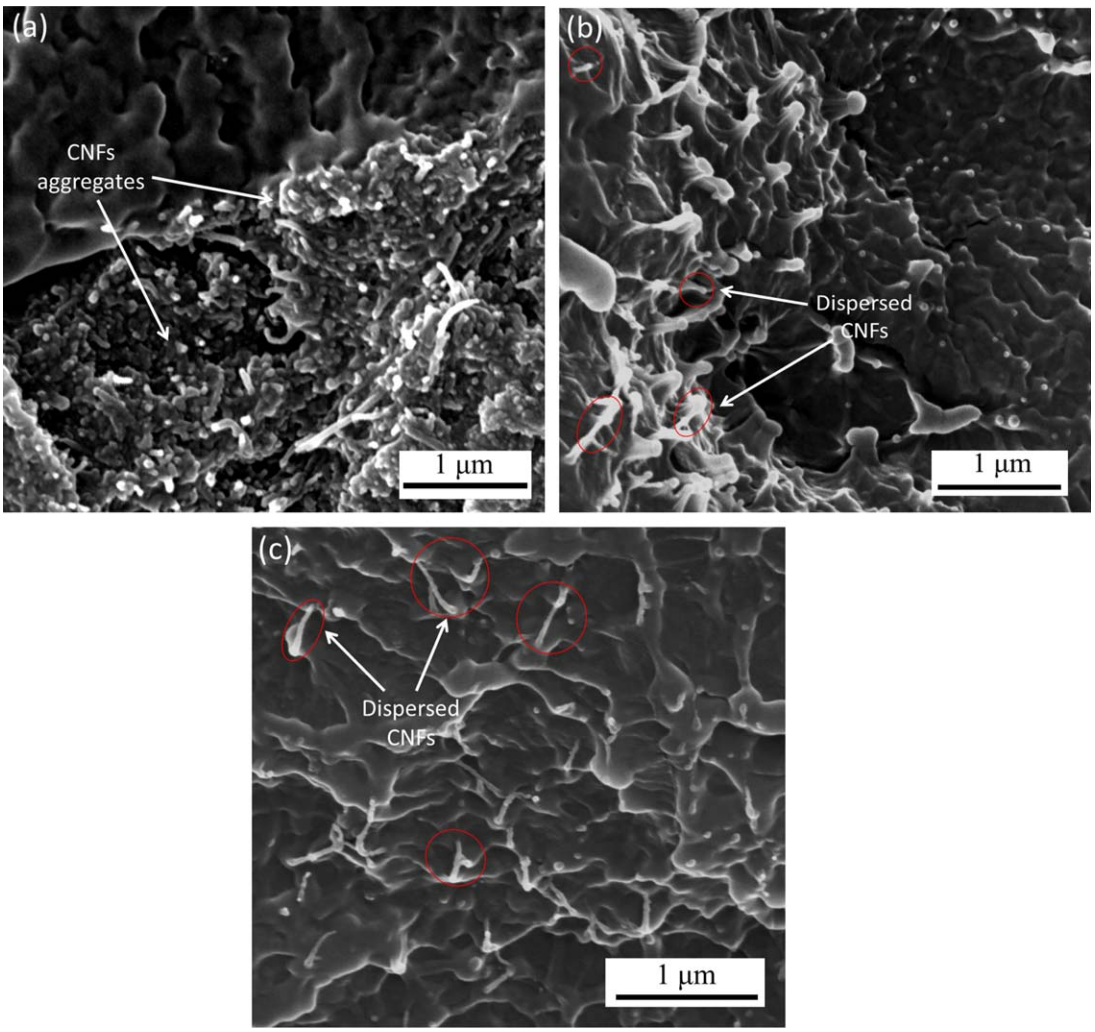

Figure 5. SEM images of the fracture surface in PA1212/CNFs composites: (a) 0.3 wt % PA1212/pristine CNFs, (b) 0.3 wt % PA1212/CNF-*g*-EDA, and (c) 0.3 wt % PA1212/CNF-*g*-PEI. [Color figure can be viewed in the online issue, which is available at wileyonlinelibrary.com.]

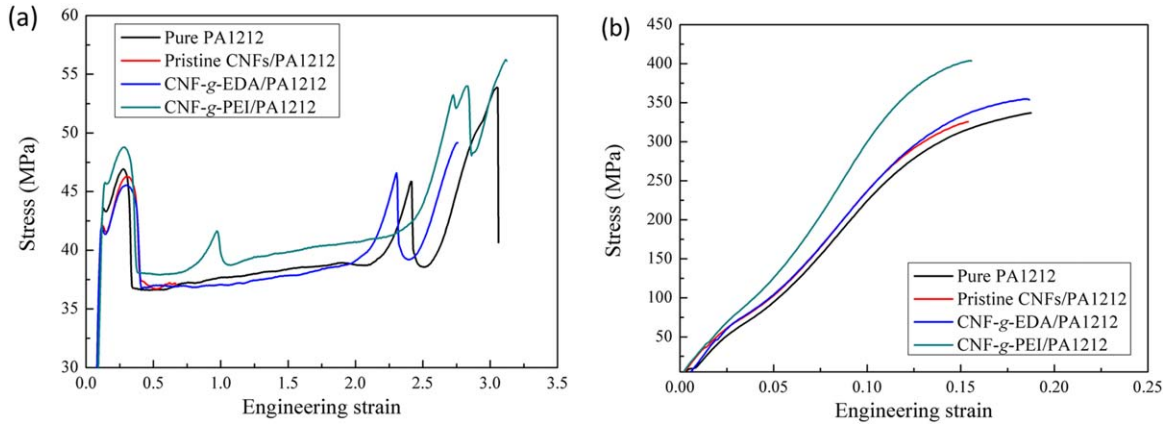

Figure 6. Mechanical properties of PA1212 composites containing 0.3 wt % CNFs: (a) undrawn samples, and (b) drawn samples. [Color figure can be viewed in the online issue, which is available at wileyonlinelibrary.com.]

performance of the PA1212/CNF-*g*-EDA composite is better compared with PA1212/pristine CNFs composite. For undrawn PA1212/CNF-*g*-PEI composite, the mechanical properties are enhanced slightly compared with pure PA1212 (as show in Table I). Thereby, the surface modification of CNFs is essential for enhancement of mechanical properties.

The mechanical properties of the drawn pure PA1212 and the composites are shown in Figure 6(b). For pure PA1212, the tensile strength is improved from 54 to 337 MPa after drawing. Improvement of mechanical properties of pure PA1212 can be ascribed to the polymer chain orientation and deformation induced crystallization.[30,31] For drawn PA1212/pristine CNFs composite, the Young's modulus is improved and the tensile strength decreases slightly compared with pure PA1212. The tensile strength of the PA1212/CNF-*g*-EDA composite is improved to 354 MPa, higher than 337 MPa for pure PA1212. Specially, the reinforcement of the PA1212/CNF-*g*-PEI composite is more effective. The tensile strength of the PA1212/CNFs-*g*-PEI composite is improved to 404 MPa, and it reaches relatively high value in all the samples. The mechanical properties of the composites are efficiently reinforced with the addition of modified CNFs after drawing, especially for PA1212/CNF-*g*-PEI composite. To further analyze the reinforcing effect, the influence of surface modification of CNFs on crystallization properties and structure orientation will be discussed as follows.

Crystallization Behavior of Pure PA1212 and PA1212/CNFs Composites

In polymer composites, different surface modification of CNFs results in different compatibility and interfacial adhesion, which influences the crystallization behavior inevitably.[8] The effect of CNFs on the crystallization behavior of PA1212/CNFs composites was analyzed by non-isothermal DSC experiments (Figure 7 and Table II). The crystallinity (X_c) is determined as the ratio of the integrated heat of fusion value of the sample over the heat of fusion of purely crystalline PA1212,

$$X_c = \frac{\Delta H_m \times 100}{\Delta H_m^o} \quad (3)$$

where ΔH_m and ΔH_m^o are the enthalpy of fusion of samples and the equilibrium melting enthalpy, respectively. The ΔH_m^o value for PA1212 is 292.2 J g^{-1}.[32] The X_c values calculated are shown in Table I.

As shown in Figure 7(b,d), CNFs show efficient heterogeneous nucleation effect during crystallization of the composites. With the addition of 0.3 wt % CNFs, the crystallization onset temperature ($T_{c,o}$) and peak temperature ($T_{c,p}$) increase by ~7°C and ~4°C, respectively. The melting points of PA1212/CNFs composites are higher than those of pure PA1212 after drawing [Figure 7(c)]. In addition, a double-melting behavior is observed in the composites. The first melting peak is at ~192°C and the second

Table I. The Mechanical Properties of Pure PA1212 and the Composites

	Samples	Tensile strength (MPa)	Yield strength (MPa)	Young's modulus (MPa)	Elongation at break (%)
Undrawn	Pure PA1212	53.8 ± 2.5	47.0 ± 0.4	527.4 ± 10.6	305.6 ± 25.3
	pristine CNFs/PA1212	46.3 ± 0.5	46.3 ± 0.6	522.3 ± 11.7	67.3 ± 4.0
	CNF-*g*-EDA/PA1212	49.2 ± 2.2	45.5 ± 0.3	542.4 ± 20.2	276.0 ± 53.4
	CNF-*g*-PEI/PA1212	56.3 ± 2.0	48.8 ± 0.5	537.5 ± 24.2	311.8 ± 11.2
Drawn	Pure PA1212	336.9 ± 11.8	–	1759.8 ± 79.9	18.8 ± 1.0
	pristine CNFs/PA1212	326.4 ± 7.9	–	1815.0 ± 92.2	15.4 ± 0.4
	CNF-*g*-EDA/PA1212	354.0 ± 5.0	–	1930.1 ± 77.5	18.5 ± 0.9
	CNF-*g*-PEI/PA1212	403.8 ± 26.5	–	2383.6 ± 198.7	15.5 ± 0.2

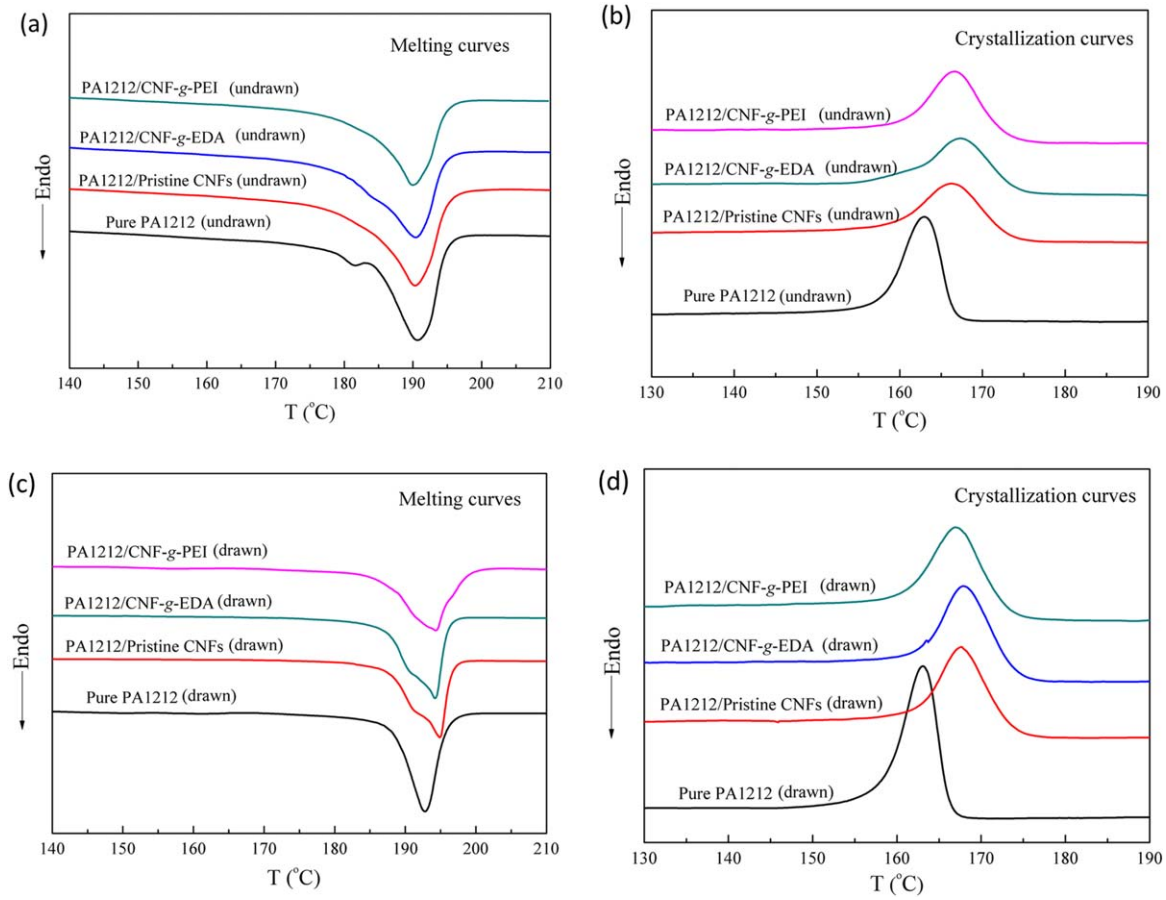

Figure 7. Non-isothermal DSC scans of pure PA1212 and 0.3 wt % PA1212/CNFs composites. For undrawn samples: (a) melting curves, and (b) crystallization curves. For drawn samples: (c) melting curves, and (d) crystallization curves. [Color figure can be viewed in the online issue, which is available at wileyonlinelibrary.com.]

melting peak is higher than the first by ~2°C. The upshift of the melting temperature is ascribed to oriented crystal structures induced by CNFs during the drawing process.[33]

For undrawn samples, the crystallinities of the composites increase slightly due to the heterogeneous nucleation effect of CNFs (Table II). The crystallinities of the pure PA1212 and PA1212/CNFs composites increase significantly after drawing. In the pure PA1212 and the composites, orientation induced crystallization occurs during the drawing process. The structure evolution is observed in fiber spinning commonly,[30,31] and the enhancement of mechanical properties is ascribed to the improvement of crystallinity and degree of polymer chain orientation.[24] However, for drawn composites, crystallinities decrease slightly with the addition of CNFs, possibly because of the hindering phenomena from carbon nanofibers.[34]

WAXD Analysis of Pure PA1212 and PA1212/CNFs Composites

The 2D-WAXD patterns of the isotropic and oriented samples are shown in Figure 8. Before drawing, the WAXD patterns exhibit several Debye−Scherrer rings that are typical in isotropic

Table II. DSC Analysis of Pure PA1212 and 0.3 wt % PA1212/CNFs Composites

	Samples	$T_{m,p}$ (°C)	$T_{c,o}$ (°C)	$T_{c,p}$ (°C)	X_c (%)
Undrawn	Pure PA1212	190.3	166.4	163.0	12.08
	Pristine CNFs/PA1212	190.3	173.1	166.3	13.51
	CNF-g-EDA/PA1212	190.4	173.8	167.3	12.31
	CNF-g-PEI/PA1212	189.9	172.5	166.8	14.20
Drawn	Pure PA1212	192.7	166.1	163.1	21.88
	Pristine CNFs/PA1212	194.8	173.4	167.7	17.72
	CNF-g-EDA/PA1212	194.2	173.9	167.9	19.67
	CNF-g-PEI/PA1212	194.3	172.9	167.0	20.12

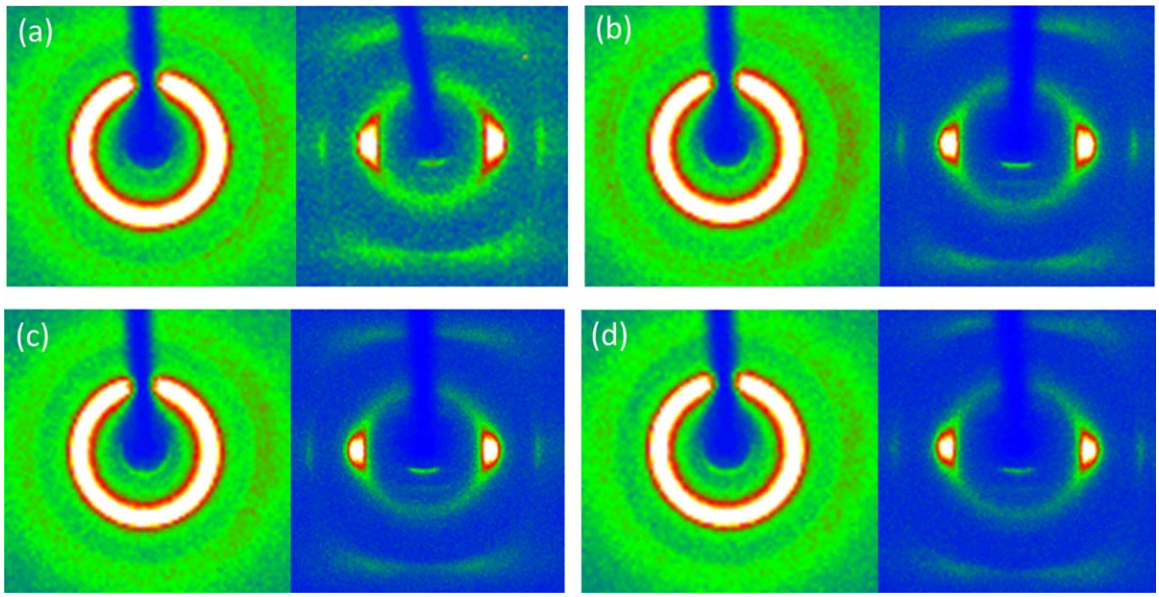

Figure 8. The 2D-WAXD patterns of the samples: (a) pure PA1212, (b) 0.3 wt % PA1212/pristine CNFs, (c) 0.3 wt % PA1212/CNF-*g*-EDA, (d) 0.3 wt % PA1212/CNF-*g*-PEI (the drawing direction is vertical). [Color figure can be viewed in the online issue, which is available at wileyonlinelibrary.com.]

diffraction. For the samples drawn at high temperature, the reflection of crystal plane moves toward the equator directly and the sharp maxima for (100) and (010/110) reflection is observed (as shown in Figure 8).

The α- and γ-crystal forms can coexist in the same crystallite of PA1212.[32] As shown in Figure 9, two distinct peaks are observed in all of the samples; these peaks correspond to the (100) and (010/110) crystal planes. Thus, PA1212 crystallizes in the triclinic α-form dominantly, and the (010/110) crystal plane is the characteristic α-crystal form. The (010) crystal plane consists of sheets of hydrogen-bonded chains formed between parallel chains, and this plane has the priority growth.[35] For pure PA1212, the relative diffraction intensity of (010/110) crystal plane increases obviously after drawing, which indicates that the drawing process induces the formation of α-crystal form. After the addition of CNFs, the relative diffraction intensity of (010/110) crystal plane of the composites decreases with respect to that of the (100) crystal plane, especially for CNF-*g*-PEI. The presence of CNFs facilitates the formation of less-ordered γ-crystal form after drawing. This result is consistent with the results of PA6/clay nanocomposites, in which the addition of nanoclay filler induces the formation of γ-crystal form.[36,37]

Based on the 2D-WAXD patterns (Figure 8), the orientation degree is calculated from (100) crystal plane scattering signal by Herman's orientation function (Formula 1 and 2). The degree of crystal orientation of the composites increases with the incorporation of CNFs (Table III). Melt-recrystallization occurs when the drawing temperature approaches the melting temperature and the 380% engineering strain is in the strain-hardening stage.[38,39] According to literature reports, the heterogeneous nucleation and template effects of aligned nanofibers on oriented crystalline structure are effective for the drawn polymer composites.[18,19] The lamellae grow epitaxially on the CNFs surface through melt-recrystallization during the drawing process.

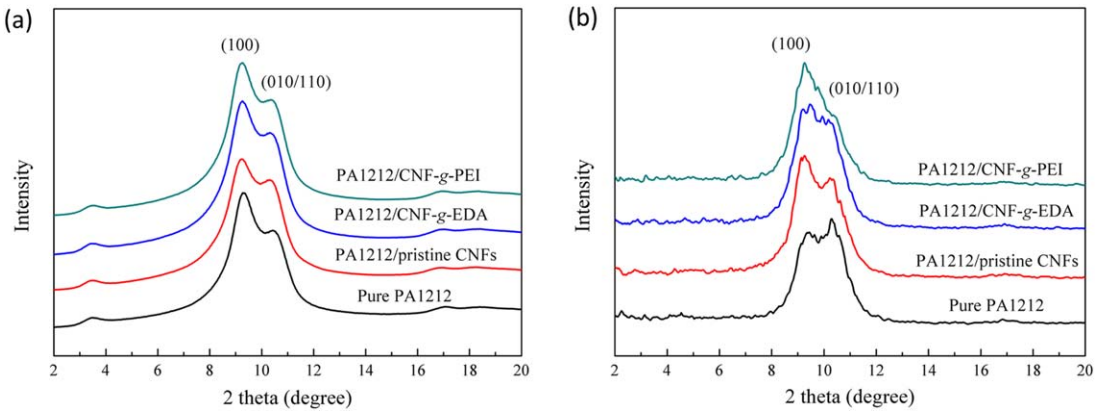

Figure 9. 1D-WAXD curves taken along the drawing direction based on 2D-WAXD patterns: (a) the undrawn samples, and (b) the drawn samples. [Color figure can be viewed in the online issue, which is available at wileyonlinelibrary.com.]

Table III. Degree of the Crystal Orientation of Pure PA1212 and 0.3 wt % PA1212/CNFs Composites After Drawing

Samples	Pure PA1212	PA1212/ pristine CNFs	PA1212/ CNF-*g*-EDA	PA1212/ CNF-*g*-PEI
Orientation degree	0.78	0.87	0.88	0.89

When the PA1212/CNFs composites have higher crystallization temperature [Figure 7(b)], the melt-recrystallization process of the composites is more complete in the limited drawing period (at 170°C for 5 min) compared with that of the pure PA1212. In addition, the crystals are more perfect and fewer polymer chains relax. Thus, the composites exhibit higher crystal orientation degree than pure PA1212 after drawing. Meanwhile, as the interfacial adhesion and dispersion state are improved (referring to Raman spectrum, T_g and SEM results), the crystal orientation degree is increasing (Table III). Favorable dispersion and interfacial adhesion of CNFs in polymer matrix can prevent polymer chains from relaxing during the drawing process. The improved polymer chain orientation degree is crucial to obtain better mechanical performance. During the tensile loading, only the fibrils oriented along the loading direction experience the stretching force.[11,40] It should be noted that this reinforcement in tensile strength caused by alignment of CNFs will be limited, because the content of CNFs in the composites is very low (only 0.3 wt.%). And it can be verified by theoretical calculation based on well-known rule of mixture.[1] Consequently, the reinforcing effect of the PA1212/CNF-*g*-PEI (CNF-*g*-EDA) composites is mainly attributed to improved degree of crystal orientation compared with that of pure PA1212 after drawing.

CONCLUSIONS

This article studied the effect of CNF surface modification on the reinforcement of PA1212 composites. CNFs were successfully modified via reactive grafting with two different size molecules (EDA and PEI). The mechanical properties of the PA1212 composites were efficiently reinforced with the addition of 0.3 wt % CNFs after drawing. From SEM and Raman spectrum results, the interfacial adhesion and dispersion state of CNFs in PA1212 matrix were improved after CNF surface modification, and it resulted in improved T_g. The improved interfacial adhesion and dispersion was beneficial to reinforcement of the composites. The degree of crystal orientation in the composites was higher than that of pure PA1212 after drawing. The reinforcing effect of the drawn PA1212/CNFs (CNF-*g*-EDA and CNF-*g*-PEI) composites is mainly ascribed to improved degree of crystal orientation.

ACKNOWLEDGMENTS

The authors appreciate Xinyang Zeng for the help in Raman spectrum characterization in College of Chemical Engineering (China University of Petroleum).

REFERENCES

1. Coleman, J. N.; Khan, U.; Blau, W. J.; Gun'ko, Y. K. *Carbon* **2006**, *44*, 1624.
2. Al-Saleh, M. H.; Sundararaj, U. *Carbon* **2009**, *47*, 2.
3. Tibbetts, G. G.; Lake, M. L.; Strong, K. L.; Rice, B. P. *Compos. Sci. Technol.* **2007**, *67*, 1709.
4. Coleman, J. N.; Khan, U.; Gun'ko, Y. K. *Adv. Mater.* **2006**, *18*, 689.
5. Dzenis, Y. *Science* **2008**, *319*, 419.
6. Sahoo, N. G.; Rana, S.; Cho, J. W.; Li, L.; Chan, S. H. *Prog. Polym. Sci.* **2010**, *35*, 837.
7. Rong, H. P.; Han, K. Q.; Li, S.; Tian, Y. C. *J. Appl. Polym. Sci.* **2013**, *127*, 2033.
8. Meng, H.; Sui, G. X.; Fang, P. F.; Yang, R. *Polymer* **2008**, *49*, 610.
9. Shi, D. L.; Jie, L.; Peng, H.; Wang, L. M. *Appl. Phys. Lett.* **2003**, *83*, 5301.
10. Hasan, M. M.; Zhou, Y. X.; Jeelani, S. *Mater. Lett.* **2007**, *61*, 1134.
11. Goh, P. S.; Ismail, A. F.; Ng, B. C. *Compos. Part A Appl. S.* **2014**, *56*, 103.
12. Wang, X.; Bradford, P. D.; Liu, W.; Zhao, H. B.; Inoue, Y. K. *Compos. Sci. Technol.* **2011**, *71*, 1677.
13. Hou, Z. C.; Wang, K.; Zhao, P.; Zhang, Q. *Polymer* **2008**, *49*, 3582.
14. Minus, M. L.; Chae, H. G.; Kumar, S. *Polymer* **2006**, *47*, 3705.
15. Chae, H. G.; Minus, M. L.; Kumar, S. *Polymer* **2006**, *47*, 3494.
16. Barber, A. H.; Cohen, S. R.; Wagner, H. D. *Appl. Phys. Lett.* **2003**, *82*, 4140.
17. Liu, Y. D.; Kumar, S. *Appl. Mater. Inter.* **2014**, *6*, 6069.
18. Chen, Y. H.; Zhong, G. J.; Lei, J.; Li, Z. M.; Hsiao, B. S. *Macromolecules* **2011**, *44*, 8080.
19. Haggenmueller, R.; Fischer, J. E.; Winey, K. I. *Macromolecules* **2006**, *39*, 2964.
20. Mai, F.; Wang, K.; Yao, M. J.; Deng, H. *J. Phys. Chem. B* **2010**, *114*, 10693.
21. Yang, J. H.; Wang, K.; Deng, H.; Chen, F.; Fu, Q. *Polymer* **2010**, *51*, 774.
22. Ning, N. Y.; Fu, S.; Zhang, W.; Chen, F. *Prog. Polym. Sci.* **2012**, *37*, 1425.
23. Ren, C. Y.; Jiang, Z. Y.; Du, X. H.; Men, Y. F. *J. Phys. Chem. B* **2009**, *113*, 14118.
24. Morioka, T.; Kakiage, M.; Yamanobe, T.; Komoto, T. *Macromolecules* **2007**, *40*, 9413.
25. Cao, C. H.; Li, J. L.; Jia, Z. J.; Chen, Z. H. *New Carbon Mater.* **2004**, *2*, 138.
26. Avile's, F.; Cauich-Rodrı'guez, J. V.; Moo-Tah, L.; May-Pat, A. *Carbon* **2009**, *47*, 2970.
27. Ramanathan, T.; Fisher, F. T.; Ruoff, R. S.; Brinson, L. C. *Chem. Mater.* **2005**, *17*, 1290.
28. Endo, M.; Kim, Y. A.; Hayashi, T.; Yanagisawa, T. *Carbon* **2003**, *41*, 1941.
29. Mu, M. F.; Osswald, S.; Gogotsi, Y.; Winey, K. I. *Nanotechnology* **2009**, *20*, 335703.
30. Penning, J. P.; Ruiten, J. V.; Brouwer, R.; Gabrielse, W. *Polymer* **2003**, *44*, 5869.

31. Samon, J. M.; Schultz, J. M.; Wu, J.; Hsiao, B. S. *J. Polym. Sci. Polym. Phys.* **1999**, *37*, 1277.
32. Ren, M. Q.; Mo, Z. S.; Chen, Q. Y.; Song, J. B. *Polymer* **2004**, *45*, 3511.
33. Yang, J. H.; Wang, K.; Deng, H.; Chen, F.; Fu, Q. *Polymer* **2010**, *51*, 774.
34. Gorrasi, G.; Lieto, R. D.; Patimo, G.; Pasquale, S. D. *Polymer* **2011**, *52*, 1124.
35. Zhang, Q. X.; Mo, Z. S.; Zhang, H. F.; Liu, S. Y. *Polymer* **2001**, *42*, 5543.
36. Liu, T. X.; Liu, Z. H.; Ma, K. X.; Shen, L. *Compos. Sci. Technol.* **2003**, *63*, 331.
37. Lincoln, D. M.; Vaia, R. A. *Macromolecules* **2004**, *37*, 4554.
38. Jiang, Z. Y.; Tang, Y. J.; Men, Y. F.; Enderle, H. *Macromolecules* **2007**, *40*, 7263.
39. Jiang, Z. Y.; Tang, Y. J.; Rieger, J.; Enderle, H. *Polymer* **2009**, *50*, 4101.
40. Baji, A.; Mai, Y. W.; Wong, S. C.; Abtahi, M. *Compos. Sci. Technol.* **2010**, *70*, 703.